國 立 交 通 大 學

電子物理研究所

碩士論文

氧硒化鋅與碲硒化鋅等電性半導體之變溫載子復合機制研究

Temperature dependence of the carrier recombination mechanism in isoelectronic ZnSeO and ZnSeTe semiconductors

研究生:江偉仕

指導教授:周武清 教授

中 華 民 國 一 百 年 十 月

氧硒化鋅與碲硒化鋅等電性半導體之變溫載子復合機制研究

Temperature dependence of the carrier recombination mechanism in isoelectronic ZnSeO and ZnSeTe semiconductors

研 究 生：江偉仕　　**Student：Wei-Shin Jiang**

指導教授：周武清 教授　　**Advisor：Prof. Wu-Ching Chou**

國 立 交 通 大 學

電子物理研究所

碩 士 論 文

A Thesis

Submitted to Institute of Electrophysics

College of Science

National Chiao Tung University

in partial Fulfillment of the Requirements

for the Degree of Master

in

Electrophysics

October 2011

Hsinchu, Taiwan, Republic of China

中 華 民 國 一 百 年 十 月

氧硒化鋅與碲硒化鋅等電性半導體
之變溫載子復合機制研究

研究生:江偉仕　　指導教授:周武清 教授

國立交通大學電子物理研究所

中文摘要

本研究利用光激螢光光譜及時間解析光譜探討氧硒化鋅與碲硒化鋅等電性半導體材料載子隨著溫度變化的情形。我們發現碲硒化鋅在很寬的溫度範圍所呈現複雜的衰減路徑與拉伸函數完美的吻合。由於氧原子和碲原子電負度及原子尺寸的差異造成摻入硒化鋅後會產生不同的物理特性。隨著溫度上升，氧硒化鋅的生命期的呈現下降的趨勢與碲硒化鋅的生命期在 70K 前會先隨著溫度上升，而在 70K 之後碲硒化鋅的生命期隨溫度的上升而下降有顯著的對比。載子的復合機制與 S 型和 V 型的氧硒化鋅與碲硒化鋅的光激螢光峰值相符合。氧硒化鋅與碲硒化鋅不同的載子復合機制可以歸因於摻雜氧或碲而產生不同的能帶模型及侷限深度所導致。

Temperature dependence of the carrier recombination mechanism in isoelectronic ZnSeO and ZnSeTe semiconductors

Student: Wei-Shin Jiang Advisor: Prof. Wu-Ching Chou

Institute of Electrophysics

National Chiao Tung University

Abstract

This study investigates carrier relaxation dynamics of isoelectronic $ZnSe_{1-x}O_x$ and $ZnSe_{1-y}Te_y$ semiconductors as a function of temperature using photoluminescence (PL) and time-resolved PL spectroscopy. We find that the complex decay traces of $ZnSe_{1-y}Te_y$ correlate excellently with the stretched exponential law within a wide temperature range. As the temperature increases, the monotonically decreased PL lifetime for $ZnSe_{0.947}O_{0.053}$ is in remarkable contrast to $ZnSe_{0.950}Te_{0.050}$ whose PL lifetime initially increases up to 70 K and then declines. These findings are consistent with the S- and V-shaped PL peak shift for $ZnSe_{0.947}O_{0.053}$ and $ZnSe_{0.950}Te_{0.050}$, respectively. The dissimilar carrier dynamics can be attributed to their extremely distinct band models and trapping depths.

Acknowledgment

人生的路途上充滿無數的交叉路口，慶幸給自己這個機會走上這條路，使我載滿收穫。回顧在交大的點滴，充滿快樂的歡笑、艱辛的淚水，除了自己的努力之外也憑藉著許多人的幫助才得以順利的前進，如今得以順利完成論文，心中充滿無限的感激。

在這段交大的日子裡，首先誠摯的感謝我的指導老師周武清教授，提供學生良好研究環境，在研究上悉心的指點迷津，使我在學術知識上獲益良多，在待人處事上積極認真負責的態度更成為我學習的典範；非常感謝陳衛國老師、張文豪老師、林烜輝老師、謝振豪老師給予指導及寶貴的建議使得論文更臻完善；特別感謝彥丞學長，在各方面循序漸進指引我，對我的成長給予讚美，對錯誤的地方給予指正，使我知曉研究的態度及矯正生活上的習性。

同時也感謝實驗室的學長姐，感謝文忠學長帶領我加入實驗室並教導我實驗的方法及分享生活中的新鮮事，感謝瑞泰學長在低潮時提點我，使我得以換個想法提振精神，感謝崑峯學長在許多實驗及細節上給予意見及照顧，感謝李寧學長在百忙之餘能夠抽空教導實驗上的操作及給予研究上建議，感謝蕙璘學姐和大陸的朋友高昆為這些日子添加許多歡樂，感謝實驗室的學弟妹：維綸、侑霖、蓉霏、安傑、明叡、宣邵、嘉華和湘穎，在各方面的協助，因有你們的加入使實驗室充滿活力朝氣，研究生活的回憶因你們而豐富精彩。

此外也感謝我的朋友們，在考試的時刻感謝阿佑贊同鼓勵我，感謝阿毛和洪文不辭辛勞的替我搬家尋找住所，在低潮時感謝致瑋願意聽我發牢騷，在我失意時感謝減加能體會並協助我重新出發，感謝點心、惜兒、CC、婷婷、關燈，不僅在休憩時間帶來許多歡樂也在當我人生的課題上並給予我支持與許多明智的建議。

最後感謝我的家人，感謝爸爸這些年來的辛苦栽培及付出以及姊姊對我的支持，你們是支撐我前進最大的動力，讓我得以順利完成學業。也感謝二伯對我的關心照顧。還有感謝在人生路途中相遇的許多朋友，在成長過程中帶給我歡笑與淚水，也使我磨練心智、砥礪品行、增進智慧。謹以此篇論文表達內心中誠摯的感謝。

Contents

List of Figures

Chapter 1 Introduction

Highly mismatched alloys (HMAs) are a class of material in which the constituent anion element is partially replaced by an isoelectronic element which very dissimilar properties, such as size and electronegativity. A well-known case is that of III-V $GaAs_{1-x}N_x$ systems, in which the constituent anion As is partially replaced by electronegativity N. It has been shown that incorporating a small a amount of N leads to profound effect on optical and electronic properties of GaAs, such as giant and asymmetric band-gap bowing, significant increase (decrease) of the electron mass (mobility), the appearance of a new optical transition (E_+), nonlinear pressure dependence of the band gap and a reduced temperature dependence of the band gap [1-6]. These anomalous effects have been well explained by using band anticrossing (BAC) model.

In III-V-N system, the BAC model can be considered as an interaction of two energy states: defect state of N and the extended conduction band state of the host matrix. The interaction of the two types of states can be treated as a perturbation which leas to following eigenvalue problem:

$$\begin{vmatrix} E - E_M & V_{MN} \\ V_{MN} & E - E_N \end{vmatrix} = 0, \tag{1}$$

where E_M is the band gap of the host matrix, E_N is the N defect state relative to valence band, and V_{MN} is the parameter describing the strength of the interaction between E_N and E_M. The two solutions of the problem can be written as,

$$E_{\pm} = (E_N + E_M \pm \left[(E_N - E_M)^2 + 4V_{MN}^2\right]^{1/2}) / 2 . \quad (2)$$

It has been shown previously that the square of the matrix is proportional to the concentration. Consequently, the strength of the coupling V_{MN} can be described as:

$$V_{MN} = C_{MN} x^{1/2}, \quad (3)$$

where C_{MN} is the matrix element coupling the localized and extended stases, and x is the concentration of Nitrogen[7-8]. An interaction of these levels with the extended states strongly affects the electronic states that determine the basic electrical and optical properties of the alloys. According to the different electronegativity between incorporated isovalent elements on the anion sublattice, which introduces localized defect states sufficiently close to the conduction-band edge (CBE) or valence-band edge (VBE) of the host matrix to undergo an anticrossing interaction with the extended states of the matrix. Over past few years, the technological importance in band gap engineering of HMAs has motivated detailed studies; however, little is know about the carrier relaxation mechanisms in the unique and complex systems.

Recently, research efforts on II-VI HMAs are focused on $ZnSe_{1-x}O_x$ and $ZnSe_{1-y}Te_y$ [3-6]. The electronegativity of the incorporated O (Te) atom is much larger (smaller) than the host Se atom, the isovalent defect level with a_1 (t_2) symmetry will form near the conduction band edge (valence band edge). Thus, the optical properties of $ZnSe_{1-x}O_x$ and $ZnSe_{1-y}Te_y$ are described by the conduction-band BAC (CBAC) and valence-band BAC (VBAC) model,

respectively. In Se-rich alloys, the theoretical fitting results yield that the O level lies 0.22 eV above the CBE of ZnSe [3], while the Te level is located at ~0.1 eV above the VBE of ZnSe [6]. Moreover, it has been shown previously that the exciton binding energy of $ZnSe_{1-x}O_x$ (x = 5.3 %) and $ZnSe_{1-y}Te_y$ (y =5.0 %) are ~20 meV and ~200 meV, respectively [6、9]. These drastic differences of their physical characteristics predict that the incorporation of O and Te into intrinsic n-type ZnSe will cause complicated and extremely dissimilar optical properties, in particular their carrier relaxation dynamics. In this thesis, we report the results of our studies on the carrier relaxation dynamics of $ZnSe_{1-x}O_x$ (x = 5.3 %) and $ZnSe_{1-y}Te_y$ (y =5.0 and 10.0 %) by using photoluminescence (PL) and time-resolved PL (TRPL) spectroscopy. The aim of this research is to compare the decay dynamics between these two ZnSe-based alloys as a function of temperature. In contrast to our previous results of $ZnSe_{1-x}O_x$ [6], we find that as the temperature increases, $ZnSe_{1-y}Te_y$ exhibits a clear discernible effect on the PL lifetime.

This thesis is organized as follows. This chapter introduces the physical properties of HMAs and BAC model. Chapter 2 introduces the PL and TRPL systems used in this thesis. In chapter 3, we report the results of our studies on the carrier relaxation mechanisms of $ZnSe_{1-x}O_x$ (x = 5.3 %) and $ZnSe_{1-y}Te_y$ (y =5.0 and 10 %). Finally, Chapter 4 summarizes this thesis.

Chapter 2 Experimental Setup

In this chapter, the experimental systems used in this thesis are described. The experimental systems include photoluminescence (PL) system and time-resolved photoluminescence (TRPL) system.

2.1 Photoluminescence (PL) System

The experimental setup of the PL system is shown in Figure 2.1. The samples were loaded on the cold finger of a closed cycle cryostat and the temperature was controlled between 10 and 300K. The GaN pulsed (405 nm) was used as an excitation source with the excitation power of about 2mW. The incident laser beam was focused on the sample by a convex Lens (L1). The PL signal from the sample was collected by a set of convex lenses (L2 and L3) and guided to spectrometer. The signal was dispersed by an iHR550 spectrometer and detected by liquid nitrogen cooled charge-coupled device (CCD). The spectrometer was controlled by a computer, which was used to store and plot the collected data.

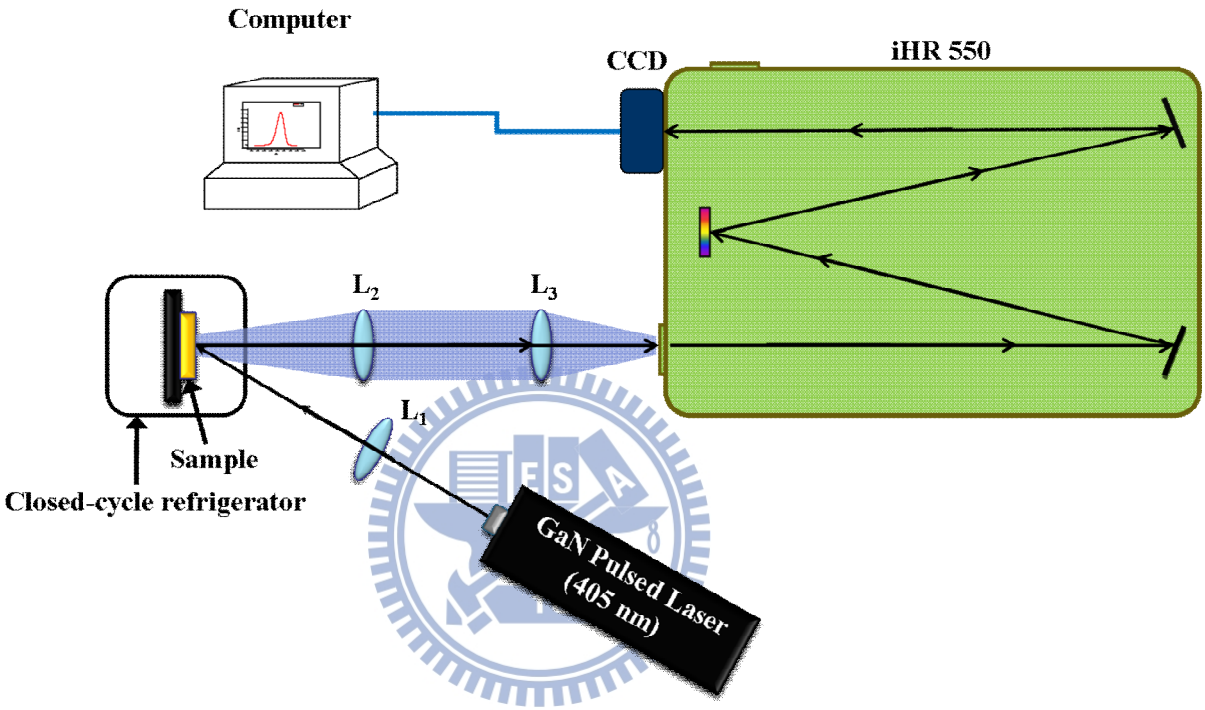

Fig. 2.1. Experimental setup of PL system.

2.2 Time-Resolved Photoluminescence (TRPL) System

TRPL system was used to study the decay dynamics of excitons. The experimental setup of TRPL system is similar to the PL system and shown in Figure 2.2. The GaN pulsed laser (405nm) with pulsed width of 200 ps and repetition rate of 2.5MHz was used as an excitation source. The laser beam was focused on the sample by convex lens (L1). The combination lenses (L2 and L3) guide the signal to the iHR550 spectrometer, which was equipped with a photon counting avalanche photodiode (APD) to detect the signal. The signal was further analyzed by a computer with a time-correlated single photon counting (TCSPC) method. The overall temporal resolution of TRPL measurement is about 200 ps.

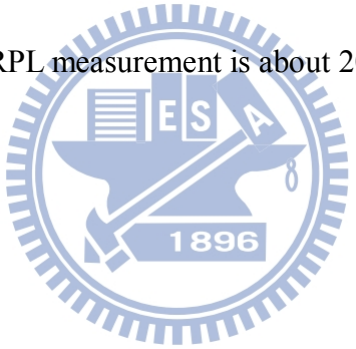

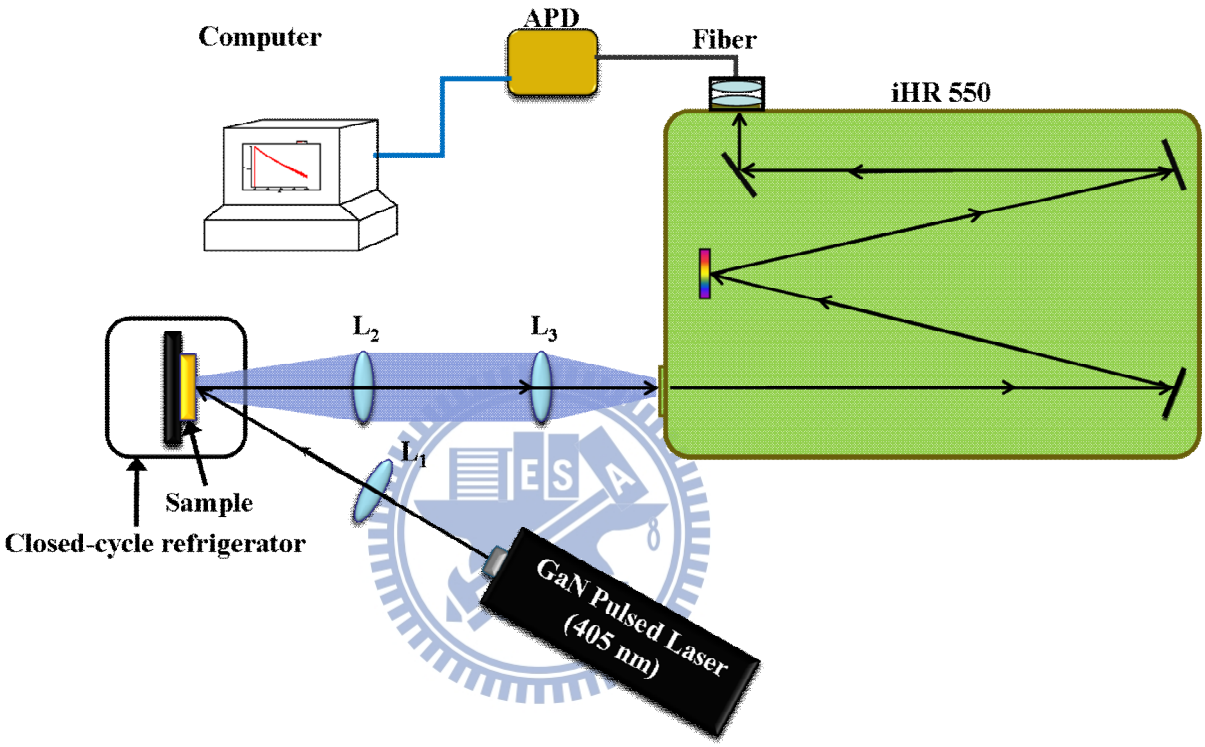

Fig. 2.2. Experimental setup of TRPL system.

Chapter 3 Result and Discussion

In this chapter, we study the carrier relaxation mechanisms of $ZnSe_{1-x}O_x$ (x = 5.3 %) and $ZnSe_{1-y}Te_y$ (y =5.0 and 10 %) using PL and TRPL measurements. The temperature of decay dynamics of $ZnSe_{1-x}O_x$ and $ZnSe_{1-y}Te_y$ will be investigated.

Figures 3.1(a)-3.1(d) show the temperature dependence of the full width at half maximum (FWHM), PL peak position, integrated PL intensity, and PL lifetime of $ZnSe_{0.947}O_{0.053}$, respectively. The FWHM increases with increasing temperature, forming a sharp peak between 60 and 130 K, where the PL peak energy undergoes a blueshift by as much as 30 meV relative to the initial rapid redshift. The concurrence of the band broadening and the S-shaped energy shift is typical for a carrier localization effect, which is explained by thermal-activated electron transfer between the localized and free states owing to the small (~ 20 meV) PL binding energy [Fig. 3.1(b)]. In Figs. 3.1(c) and 3.1(d), when the temperature exceeds 10 K, the PL intensity and lifetime decrease sharply. We note that the 10 - 80 K temperature range exhibiting the strongest thermal quenching of PL intensity and lifetime is coincident with the temperature region exhibiting the strongest PL redshift and linewidth broadening. These experimental findings are most likely due to the increased nonradiative recombination rate at higher temperatures where thermal-activated electrons hop to deeper O traps.

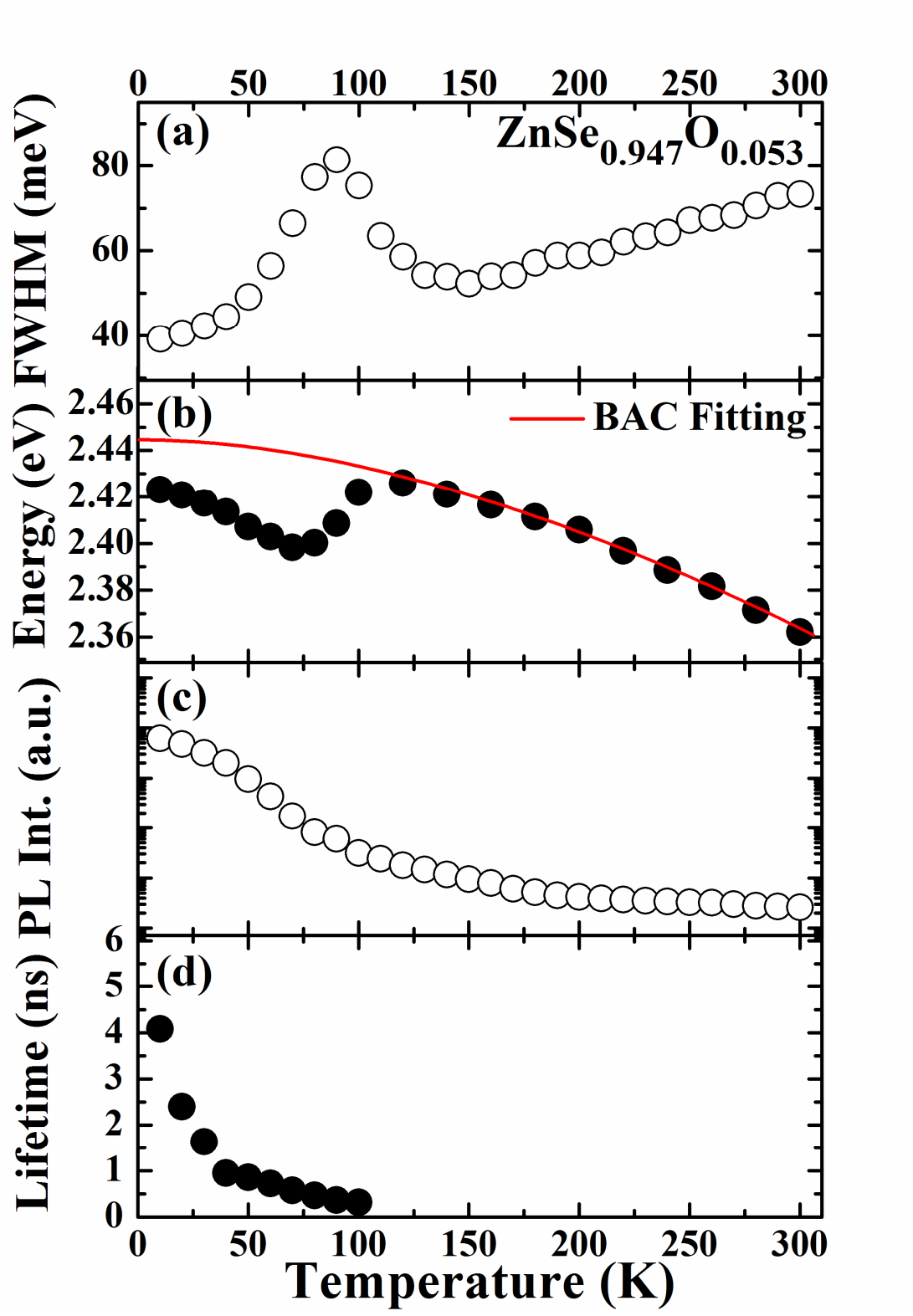

Fig. 3.1 Temperature-dependent (a) FWHM (b) PL peak energy (c) integrated PL intensity (d) PL Lifetime of $ZnSe_{0.947}O_{0.53}$. Solid line in (b) represents fit using BAC model.

Figure 3.2(a) shows the temperature-dependent PL spectra for $ZnSe_{0.950}Te_{0.050}$ from 10 to 300 K along with indicated peak positions. The PL peaks exhibit a V-shaped energy shift as the temperature increases. At low temperatures (< 140 K), the PL emissions shift monotonically toward lower energies, which shift is accompanied by asymmetric linewidth broadening with increasing temperature. As the temperature further increases above 140 K, a pronounced blueshift of this peak is observed and a high energy shoulder appears. Figure 3.2(b) plots the temperature-dependent PL peak energies obtained from Fig. 3.2(a). In comparison with the S-shaped energy shift of $ZnSe_{0.947}O_{0.053}$, the V-shaped energy shift herein implies a quite deep trap resulted from alloy fluctuations or Te clustering. From the PLE spectrum of $ZnSe_{0.950}Te_{0.050}$ detected at the PL peak and 10 K, it is clear that this emission is preferentially excited via band-to-band processes. Moreover, a large Stokes shift of ~ 200 meV with respect to the band edge measured by PLE is observed. The value agrees well with the PL binding energy ($E_g - E_{PL}$) obtained previously using photoconductivity and reflectivity approaches [9], indicating that the emissions within the temperature range are all generated by localized excitons. Above 140 K, the peak energy initially undergoes a slow blueshift up to 260 K and then a fast shift until 300 K. The phenomena can be understood via different decay channels shown in the inset of Fig. 3.2(b), which will be discussed in details later.

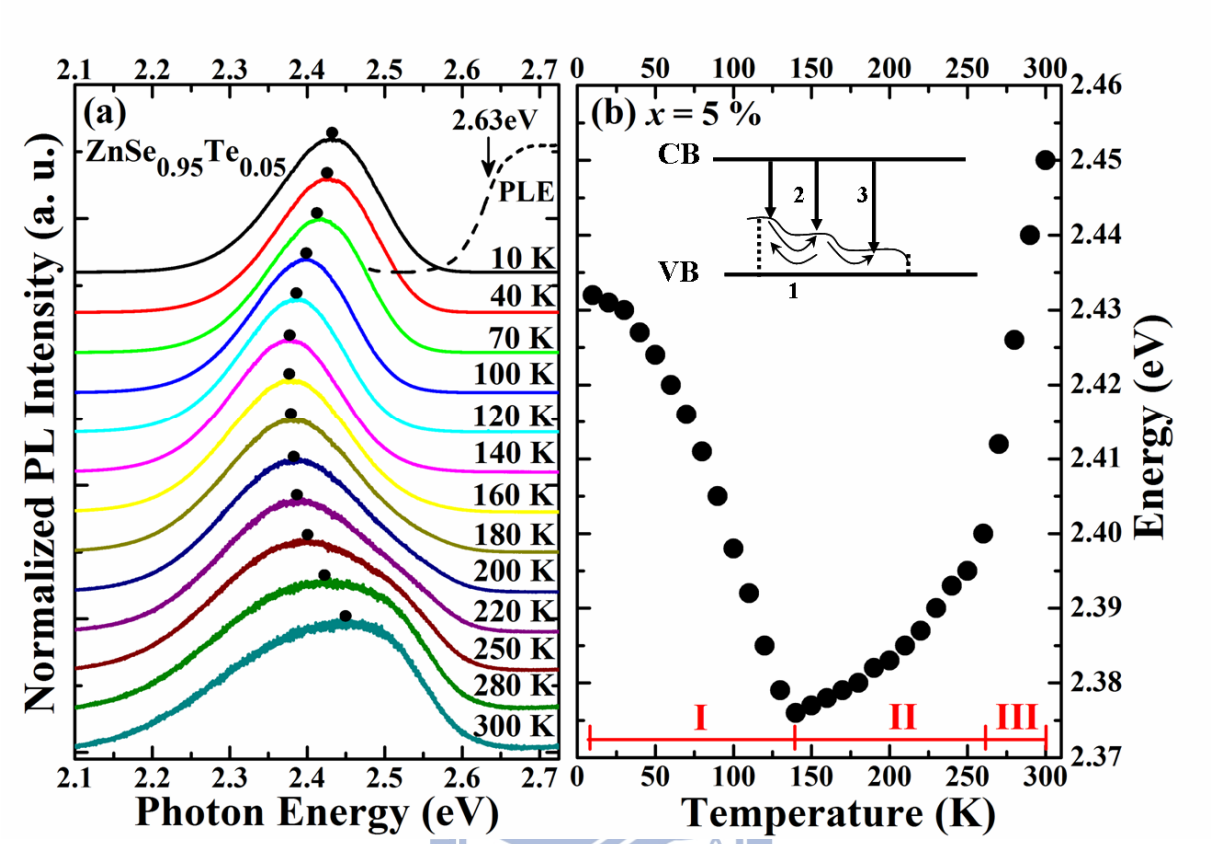

Fig. 3.2 (a) Temperature-dependent PL spectra of $ZnSe_{0.95}Te_{0.05}$ and (b) corresponding PL peak energy against temperature. Dashed curve in (a) represents the PLE spectrum of $ZnSe_{0.950}Te_{0.050}$ detected at the PL peak and 10 K. Inset in (b) shows schematic diagram of carrier decay paths and only three trap states are considered for simplicity.

To gain insight into the carrier relaxation dynamics of $ZnSe_{0.950}Te_{0.050}$, Fig. 3.3(a) shows the temperature-dependent TRPL spectra. Clearly, several interesting conclusions can be drawn. (i) As the temperature increases, the PL lifetime initially increases up to 70 K and then monotonically declines. (ii) None of the PL decay profiles behave in a monoexponential decay. (iii) All of the TRPL spectra on a double logarithmic scale exhibit straight lines [inset in Fig. 3.3(a)], which are strong evidences that the PL decay profiles of $ZnSe_{0.950}Te_{0.050}$ follow the stretched exponential law. These facts indicate a peculiar and complex carrier decay mechanism in $ZnSe_{0.950}Te_{0.050}$. Accordingly, the decay curves of $ZnSe_{0.950}Te_{0.050}$ are all fitted using the stretched exponential function, $I(t) = I_0 \cdot e^{-(t/\tau)^{\beta}}$, where β is the stretching exponent ($0 < \beta \leqq 1$) and τ is the PL lifetime. The β reflects the relaxation rates involved in the decay process, in which a broader rate distribution causes a smaller β. The gradient of the double natural logarithm versus the natural logarithm yields the variation of β.

Figures 3.3(b) and 3.3(c) plot the measured τ and β against temperature for $ZnSe_{0.950}Te_{0.050}$. In contrast with τ, β initially decreases to a minimum at 140 K and then monotonically increases with a further increase in temperature. It is worth mention that the turning point of β at 140 K correlates well with that of the PL peak energy shown in Fig. 3.2(b). The phenomenon can be explained by the configuration coordinate diagram shown in the inset of Fig. 3.2(b). At 10 K, holes hop among adjacent transport and trapping sites and then are tightly bound to the most numerous trap states. However, electrons are more weakly

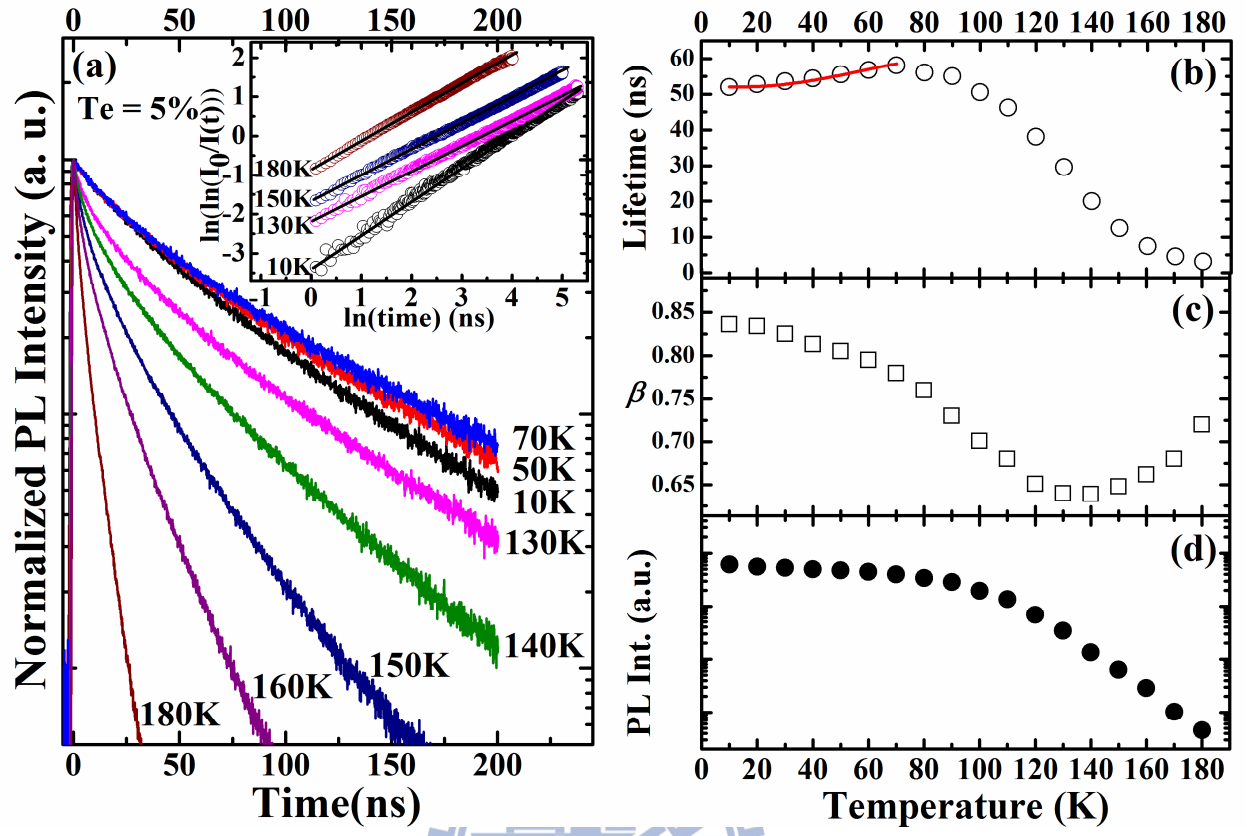

FIG. 3.3 Temperature-dependent (a) TRPL spectra, (b) PL lifetime, (c) stretching exponent, and (d) integrated PL intensity of $ZnSe_{0.950}Te_{0.050}$. Inset in (a) shows the TRPL spectra on a double logarithmic scale.

bound by a Coulomb force, giving rise to the excitons and subsequently recombine. As the temperature increases, the holes gain additional energy to hop toward deeper traps (path I), causing a redshift of the PL emission energy and a reduction of β. Around 140 K the decay dynamics becomes complicated, part of the holes are thermally activated toward higher energy states. Consequently, PL linewidth broadens at the high energy shoulder, and the values of both PL peak energy and β reach their local dip. Above 140 K most of the holes gain sufficient energy to repopulate back to the high energy states (path II) and recombine, leading to the blueshift in the PL peaks and an increase in β. Increasing the temperature further above 260 K, a sharp energy blueshift is observed (path III). It is because holes suddenly mobilize up to higher Te traps with dissimilar energy from that in path II.

An initial increase in τ shown in Fig. 3.3(b) can be readily understood as follows. In $ZnSe_{0.950}Te_{0.050}$, holes hop among proximal Te traps and remain much tighter bound than electrons. As the temperature rises, electrons tend to achieve an equilibrium distribution between the positively charged Te traps and the conduction band. Accordingly, the weakly bound electrons are ionized and away from the strongly localized holes for an increasing fraction of their lifetimes, which in turn will lengthen the radiative PL lifetime. We note that such an explanation is valid provided that the nonradiative processes are negligible, which is confirmed by the almost constant PL intensity in the same temperature region [Fig. 3.3(d)]. The temperature dependence of τ is fitted using the following equation:

$$\tau = \tau_0 / [1 - C \exp(-\varepsilon_{e-h} / kT)], \quad (1)$$

where τ_0 is the decay time at $T = 0$ K, C is a constant, $\varepsilon_{e\text{-}h}$ is a characteristic energy that is of the order of the electron-hole (*e*-*h*) binding energy, and k is the Boltzmann constant. In Fig. 3(b) the solid line is the fitting result within the temperature range where the PL intensity remains relatively constant, *i.e.*, where nonradiative processes are negligible, and it yields $\varepsilon_{e\text{-}h}$ ~ 9 meV. Such a low *e*-*h* binding energy in the temperature range correlates closely with the increasing τ due to thermal ionization of electrons.

As can be seen in Figs. 3.4(a)-4(e), similar experimental results are also found in $ZnSe_{0.900}Te_{0.100}$. Clearly, a higher Te content (y = 10 %) in $ZnSe_{1-y}Te_y$ is associated with a higher rate at which the τ increases with temperature. Fig. 3.4(a) displays the temperature-dependent TRPL spectra. In Fig. 3.4(b), a fit of the experimental data to Eq. (1) yields $\varepsilon_{e\text{-}h}$ ~ 5 meV which is lower than that of $ZnSe_{0.950}Te_{0.050}$. This is because increasing the number of Te traps, providing alternate decay routes for holes [4], causing an increased PL peak redshift at high temperatures, and decreasing the *e*-*h* binding energy due to broader distribution of localized holes. In Fig. 3.4(c), the turning point of β at 160 K agrees excellently with that of the V-shaped PL peak energy shown in Fig. 3.4(d), which again implies complex and distinct carrier dynamics at both sides around 160 K. Figures 3.5(a) and 3.5(b) show the TRPL images of $ZnSe_{0.900}Te_{0.100}$ at 10 and 180 K, respectively. At 10 K, the emission peak dramatically shifts toward the lower energy as time elapses. However, the

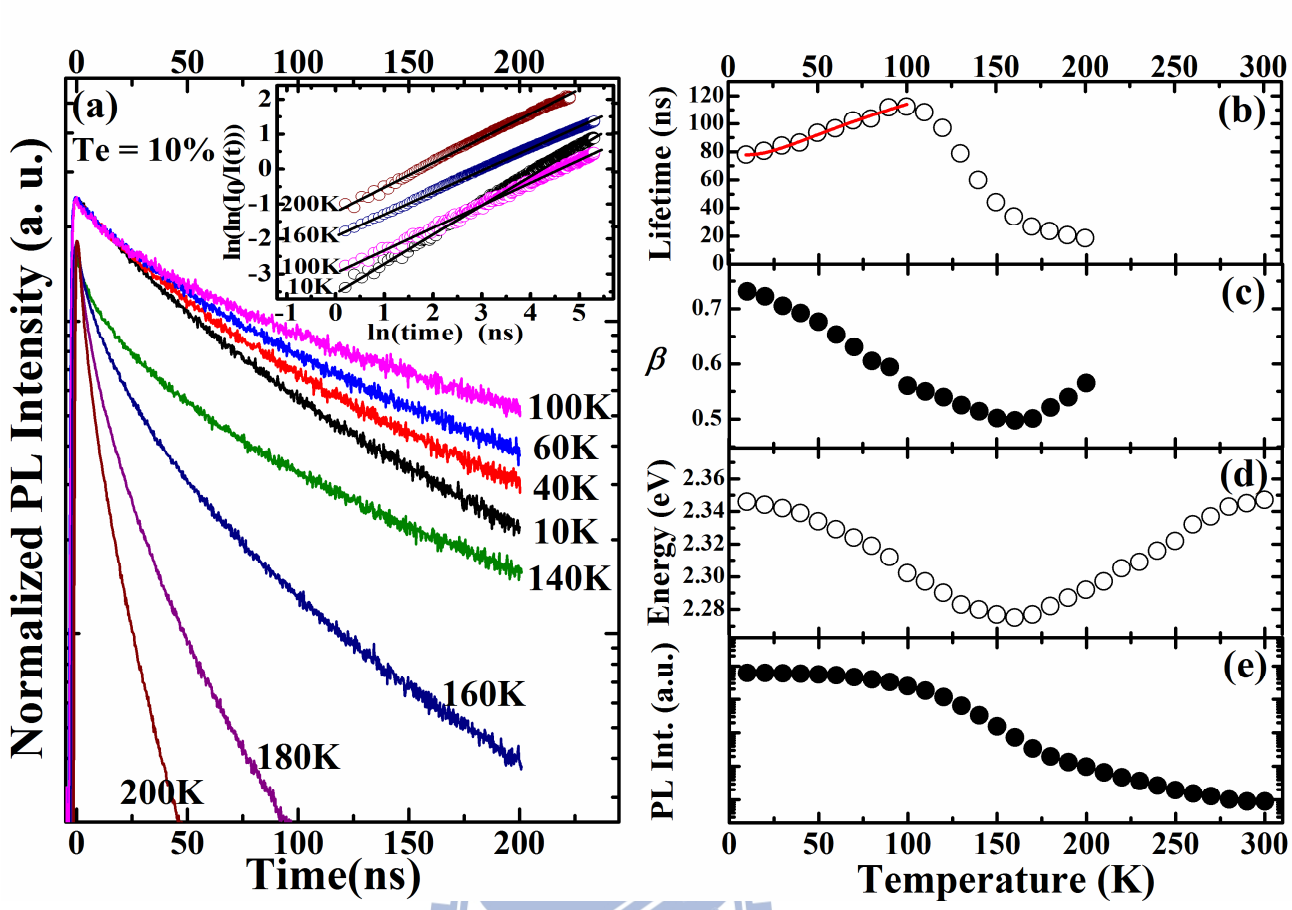

FIG. 3.4 Temperature-dependent (a) TRPL spectra, (b) PL lifetime, (c) stretching exponent, (d) PL peak energy, and (e) integrated PL intensity of $ZnSe_{0.900}Te_{0.100}$. Inset in (a) shows the TRPL spectra on a double logarithmic scale.

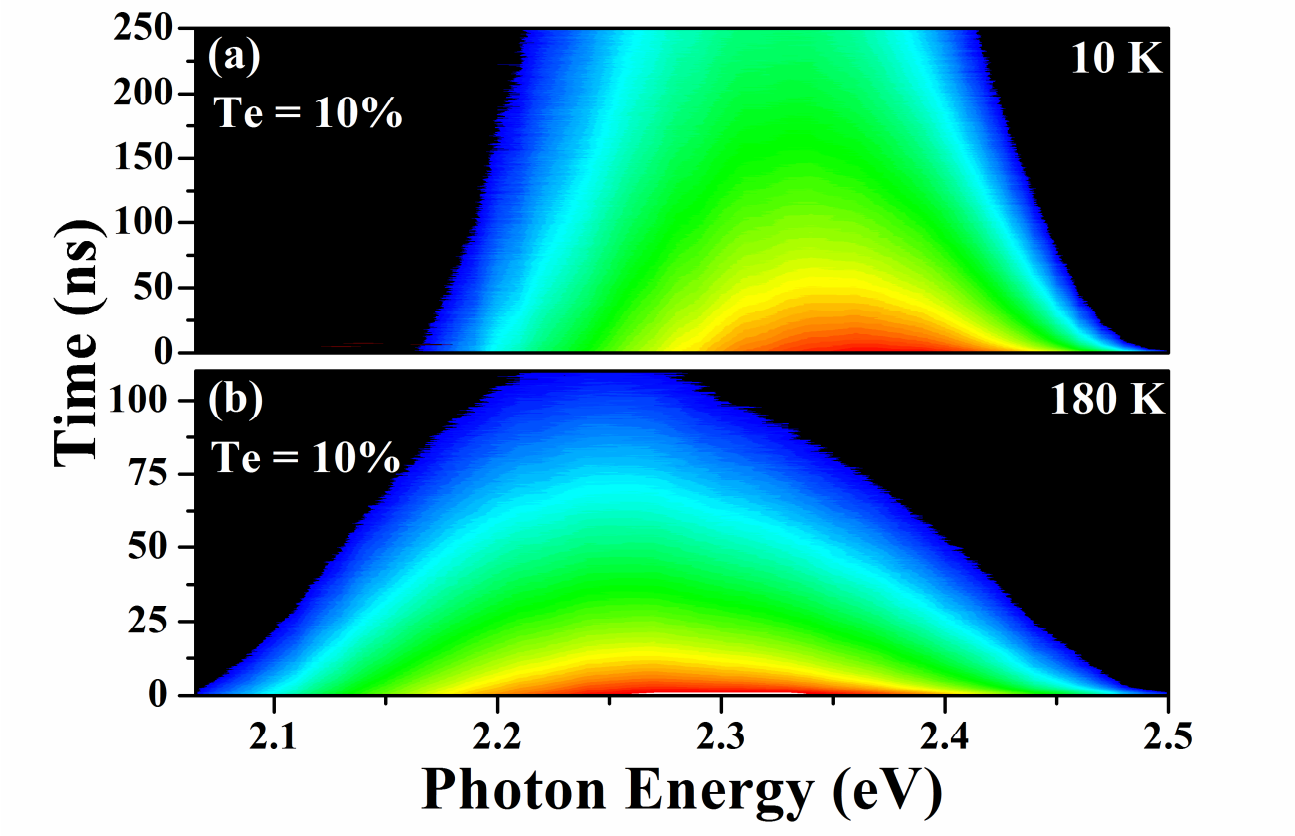

Fig 3.5 TRPL images of $ZnSe_{0.900}Te_{0.100}$ monitored at (a) 10 K and (b) 180 K.

emission redshift gradually disappears and starts shifting toward higher energies at 180 K.

Compared the carrier dynamics of $ZnSe_{0.947}O_{0.053}$ with $ZnSe_{0.950}Te_{0.050}$, we find several dissimilarities. (i) The PL peak energy of $ZnSe_{0.947}O_{0.053}$ exhibits an S-shaped shift against temperature, while that of $ZnSe_{0.950}Te_{0.050}$ displays a V-shaped shift. (ii) With similar concentration but different isovalent atoms, τ of $ZnSe_{0.947}O_{0.053}$ is smaller than that of $ZnSe_{0.950}Te_{0.050}$ at 10 K. (iii) As the temperature rises, the PL intensity and lifetime of $ZnSe_{0.947}O_{0.053}$ decrease monotonically. Similar results were also found in InGaAs:N [10] and GaAs:Bi [11] HMAs. However, τ of $ZnSe_{0.950}Te_{0.050}$ initially increases with an almost constant PL intensity and then declines. Interestingly, this type of behavior was also observed for GaN:As [12] and ZnTe:O [13] HMAs. These remarkable inconsistencies can be attributed to their distinctly different localization strengths (~ 20 meV for $ZnSe_{0.947}O_{0.053}$ and ~ 200 meV for $ZnSe_{0.950}Te_{0.050}$). Based on the BAC model, the variations are associated with different depths of the isovalent O(Te) traps relative to the energy min.(max.) of the new $E_-(E_+)$ subband. We point out that there is a clear systematic in the behavior of τ against temperature for the series ZnSe:O, InGaAs:N, GaAs:Bi, ZnSe:Te, GaN:As, and ZnTe:O. Considering the defect level positions as determined by the BAC model, we obtain for the previous series 0.22 and 0.30 eV above CBE, 0.40 eV below VBE, 0.10 and 0.62 eV above VBE, and 0.24 eV below CBE, respectively [1,3,5,6,14,15]. It might indicate for defect levels outside the band gap, the anticrossing interaction results in the formation of a relatively wide lower (higher) E_-

(E_+) subband, as a result, τ decreases monotonically with temperature owing to shallower localization depth. Otherwise, for defect levels inside the band gap, a deeper trapping depth results in an initially increased τ.

Chapter 4 Conclusions

In summary, we have shown that $ZnSe_{0.947}O_{0.053}$ and $ZnSe_{0.950}Te_{0.050}$ exhibit clear discernible effects on the carrier relaxation dynamics. For $ZnSe_{0.947}O_{0.053}$ with lower electron trapping depth, the electrons tend to thermally delocalize to free states and nonradiative centers, causing a monotonic decline in both PL intensity and lifetime with increasing temperature. In a remarkable contrast, a V-shaped energy shift along with an initial increase in τ implies that the emission of $ZnSe_{0.950}Te_{0.050}$ is generated by bound excitons in which the holes are deeply trapped. Consequently, the deduced *e-h* binding energy is ~ 9 meV for $ZnSe_{0.950}Te_{0.050}$, which correlates closely into the PL decay time against temperature.

References

[1] W. Shan, W. Walukiewicz, J. W. Ager III, E. E. Haller, J. F. Geisz, D. J. Friedman, J. M. Olson, and S. R. Kurtz, Phys. Rev. Lett. **82**, 1221 (1999).

[2] C. Skierbiszewski, P. Perlin, P. Wisniewski, W. Knap, T. Suski, W. Walukiewicz, W. Shan, K. M. Yu, J. W. Ager, E. E. Haller, J. F. Geisz, and J. M. Olson, Appl. Phys. Lett. **76**, 2409 (2000).

[3] J. Wu, W. Walukiewicz, K. M. Yu, J. W. Ager III, E. E. Haller, I. Miotkowski, A. K. Ramdas, C. H. Su, I. K. Sou, R. C. C. Perera, and J. D. Denlinger, Phys. Rev. B **67**, 035207 (2003).

[4] Y. C. Lin, W. C. Chou, W. C. Fan, J. T. Ku, F. K. Ke, W. J. Wang, S. L. Yang, W. K. Chen, W. H. Chang, and C. H. Chia, Appl. Phys. Lett. **93**, 241909 (2008).

[5] W. Shan, W. Walukiewicz, J. W. Ager III, K. M. Yu, J. Wu, E. E. Haller, Y. Nabetani, T. Mukawa, Y. Ito, and T. Matsumoto, Appl. Phys. Lett. **83**, 299 (2003).

[6] Y. C. Lin, H. L. Chung, W. C. Chou, W. K. Chen, W. H. Chang, C. Y. Chen, and J. I. Chyi, Appl. Phys. Lett. **97**, 041909 (2010).

[7] A. Lindsay, E. P. O'Reilly, Solid State Commun. 112,443 (1999)

[8] W. Walukueewicz, W. Shan, J.W. Ager III, D.R Chamberlin, E. E. Haller, J. F. Geisz, D. J. Friedman, J. M. Olson, and S.R. Kurtz, Proceedings of the 195th Electrochemical Society Meeting, Seattle, WA (The Electrochemical Soc. Inc., Pennington,

NJ,1999),Vol.99-11, p. 190

[9] M. J. S. P. Brasil, R. E. Nahory, F. S. Turco-Sandroff, H. L. Gilchrist, and R. J. Martin, Appl. Phys. Lett. **58**, 2509 (1991).

[10] R. A. Mair, J. Y. Lin, H. X. Jiang, E. D. Jones, A. A. Allerman, and S. R. Kurtz, Appl. Phys. Lett. **76**, 188 (2000).

[11] S. Yoon, M. J. Seong, B. Fluegel, A. Mascarenhas, S. Tixier, and T. Tiedje, Appl. Phys. Lett. **91**, 082101 (2007).

[12] B. Gil, A. Morel, T. Taliercio, P. Lefebvre, C. T. Foxon, I. Harrison, A. J. Winser, and S. V. Novikov, Appl. Phys. Lett. **79**, 69 (2001).

[13] J. D. Cuthbert and D. G. Thomas, Phys. Rev. **154**, 763 (1967).

[14] K. Alberi, O. D. Dubon, W. Walukiewicz, K. M. Yu, K. Bertulis, and A. Krotkus, Appl. Phys. Lett. **91**, 051909 (2007).

[15] J. Wu, W. Walukiewicz, K. M. Yu, J. D. Denlinger, W. Shan, J. W. Ager III, A. Kimura, H. F. Tang, and T. F. Kuech, Phys. Rev. B **70**, 115214 (2004).